

DIOCTAHEDRAL CORRENSITE FROM PERMIAN RED BEDS, LISBON VALLEY, UTAH

S. J. MORRISON AND W. T. PARRY

Department of Geology and Geophysics, University of Utah
Salt Lake City, Utah 84112

Abstract—Regularly interstratified chlorite/smectite (corrensite) occurs as grain coatings in marine and eolian sandstones of the Permian Cutler Formation in Lisbon Valley, Utah. Corrensite dominates the <2- μm clay size fraction along with lesser amounts of regularly interstratified illite/smectite in bleached, permeable sandstones that are interbedded with smectite-dominated arkosic, red, laterally discontinuous fluvial sandstones. Chemical and X-ray powder diffraction analyses of the corrensites show them to be di/dioctahedral with 060 spacings of 1.501 to 1.508 Å and to contain significantly higher Al:Mg ratios than more common trioctahedral types. Calculated structural formulae are: corrensite, $\text{M}_{0.6}(\text{Fe}^{3+}_{0.2}\text{Mg}_{1.6}\text{Al}_{4.6})(\text{Al}_{0.2}\text{Si}_{7.8})\text{O}_{20}(\text{OH})_{10}$; illite/smectite, $\text{M}_{1.5}(\text{Fe}^{3+}_{0.1}\text{Mg}_{1.7}\text{Al}_{2.8})(\text{Al}_{1.6}\text{Si}_{6.4})\text{O}_{20}(\text{OH})_4$; and smectite, $\text{M}_{0.9}(\text{Fe}^{3+}_{0.3}\text{Mg}_{1.2}\text{Al}_{2.8})(\text{Al}_{0.6}\text{Si}_{7.4})\text{O}_{20}(\text{OH})_4$.

Chemical similarity between the smectite and the corrensite and pervasive distribution of smectite in low-permeability shales and siltstones suggest that the smectite was a precursor of the corrensite. Three stages of mineral precipitation in the Cutler Formation have been recognized. Quartz precipitated early as grain overgrowths, followed by the formation of authigenic clay minerals, and later calcite cementation which destroyed much of the original rock fabric. Calculations show that aluminous corrensite was favored by elevated temperature (~100°C), low pH, and low dissolved silica. Local hydrothermal fluids rising along the Lisbon fault apparently permeated the Cutler red bed section and precipitated the clay minerals. The assemblage corrensite + illite/smectite in the sandstones probably formed by interaction of formation fluids with smectite and an Al-bearing phase, such as K-feldspar or kaolinite.

Key Words—Corrensite, Genesis, Illite/smectite, Interstratification, Red beds, Smectite.

INTRODUCTION

Corrensite has been determined to be a regular interstratification of chlorite/vermiculite (Bradley and Weaver, 1956), chlorite/smectite (Earley *et al.*, 1956), or chlorite/swelling chlorite (Lippman, 1954). Although the AIPEA Nomenclature Committee has not yet approved names for regular interstratifications (Bailey, 1980), any interstratified chlorite/expanding-phase mineral characterized by near integral X-ray powder diffraction (XRD) basal reflections is referred to in this report as corrensite. Octahedral sites in either or both types of layers may be fully occupied or two-thirds occupied. Corrensites may be di- or trioctahedral, but a prefix di/di or di/tri is applied if the octahedral occupancy has been determined. Di/dioctahedral corrensites have been called tosudite by Frank-Kamenetsky *et al.* (1963). Lisbon Valley corrensite is dioctahedral chlorite/dioctahedral smectite as determined by XRD analyses.

Corrensite commonly forms in hypersaline sedimentary environments (Grim *et al.*, 1960; Kopp and Fallis, 1974; Weaver *et al.*, 1982), but the rapidly growing list of corrensite occurrences (Brigatti and Poppi, 1984) suggests a less restricted genetic environment. Corrensite has been reported from clastic sedimentary rocks, apparently having formed during early (burial) diagenesis (Tompkins, 1981; Suchecki *et al.*, 1977); hydrothermally altered rocks (Furbish, 1975; Sudo and Kodama, 1957); metamorphosed pelitic rocks (Blatter

et al., 1973); metamorphosed red beds (April, 1980); marine limestones (Peterson, 1961; Bradley and Weaver, 1956); and soils (Johnson, 1964; Millot and Camez, 1963). Kubler (1973) suggested that trioctahedral corrensite is an indicator of diagenetic temperatures of 90°–100°C. Its formation is favored over smectite by high dissolved Mg and high pH (Weaver, 1984). Velde (1977) suggested that corrensite forms in normal sedimentary rocks and weathering environments, and is stable throughout the full range of clay mineral physical environments.

Most corrensites in which octahedral site occupancies have been determined are tri/trioctahedral (i.e., octahedral sites in both the chlorite and the swelling layers are fully occupied). Contact metamorphosed red shales from Montana contain di/trioctahedral corrensite in which the chlorite layers are assumed to be trioctahedral and the swelling layers to be dioctahedral (Blatter *et al.*, 1973). Di/dioctahedral corrensites occur in hydrothermally altered tuffs (Shimoda, 1969; Sudo and Kodama, 1957; Sudo and Hayashi, 1956; Sudo *et al.*, 1954; Frank-Kamenetsky *et al.*, 1963) and in argillaceous volcanoclastic rocks (Pacquet, 1968).

Corrensite in the Lisbon Valley, Utah, area dominates the <2- μm clay-size fraction of bleached, permeable marine and eolian arenites within a ~500-m-thick section of Permian Cutler Formation red beds. One of the bleached strata in the upper part of the sequence, referred to as the “sugar sandstone” by uranium pros-

pectors (Figure 1), intersects the overlying Chinle (Triassic) Formation at an angular unconformity. The Cutler sugar sandstone is thought to have been an important fluid-migration pathway as shown by uranium deposits at the base of the Chinle (Wood, 1968). Poorly sorted, coarse, red to purple fluvial arkoses interbedded with bleached strata in the Cutler Formation also contain uranium deposits.

Clay fractions of both basal Chinle conglomeratic sandstones and Cutler sugar sandstone were initially sampled to define parameters of the uranium ore-forming fluids as indicated by clay mineral assemblages. The discovery of corrensite, a relatively rare clay mineral not previously reported from the Colorado Plateau, in the sugar sandstone prompted more extensive sampling and analytical work.

Diocahedral, Al-rich corrensite in Permian red beds in Lisbon Valley, Utah, adds to the rapidly growing diversity of corrensite occurrences, compositions, and environments. The purpose of this study was to determine mineralogy and composition of interstratified clays in the Permian age Cutler red beds exposed in the Lisbon Valley area and to examine the possible origin of the corrensite.

REGIONAL GEOLOGY

Lisbon Valley is in the Paradox basin, a sequence of Pennsylvanian evaporites and carbonates, in southeastern Utah and southwestern Colorado (Figure 1). The Lisbon Valley anticline formed by vertical upwelling of a low-density salt core that began to rise in upper Pennsylvanian time and continued into the Jurassic, as determined by formational thinning over the Lisbon Valley salt anticline and over other salt anticlines in the Paradox basin. Laramide orogeny reactivated salt uplift to form the present-day salt anticlines and resulted in normal displacement along the Lisbon Valley fault (Figure 1b). At Lisbon Valley, the Moenkopi Formation, which regionally overlies the Cutler Formation, is absent due to erosion or nondeposition over the rising salt core. The Cutler and Chinle Formations are thin over the anticline, and an angular unconformity exists between the Cutler and the overlying Chinle Formation (Figure 1b).

A high-angle normal fault separates the eastern Paradox basin from the Uncompahgre highland. Arkosic sediment eroded from the Uncompahgre highland during the Late Pennsylvanian–Permian periods was deposited as thick, proximal alluvial fans of the Cutler Formation. The Cutler Formation is about 1800 m

thick at the Uncompahgre front and is composed chiefly of granitic composition boulder-conglomerates, which grade into cobble and coarse sand-size midfan and distal fan deposits that are interbedded with marine facies to the west near Moab and Lisbon Valley (Mack and Rasmussen, 1984). Fifty kilometers west of Lisbon Valley, the Cutler is dominated by clastic marine units.

The Lisbon Valley area is within the transition zone of Permian red bed sedimentation from alluvial-fan to marine-dominated stratigraphy. Marine sandstones and siltstones are interbedded with distal alluvial fan deposits on a scale of meters to several tens of meters. Marine units are evenly bedded and are characterized by continuous horizontal top and bottom contacts that can generally be traced for several km with little thickness variation. The sugar sandstone (Figure 1) is an orange-red to buff, very fine grained, well-sorted, permeable quartz arenite containing large-scale, tabular cross beds; the sandstone was interpreted by Campbell and Steele-Mallory (1979) as eolian. Reddish-orange marine siltstones form massive 0.6–6.0-m-thick beds comprised of abundant sets of small-scale ripple marks. Distal-fan, laterally discontinuous, arkosic beds in Lisbon Valley have distinctly scoured bases indicating channel-confined flow. Several uranium ore bodies occur in these fluvial Cutler arkoses.

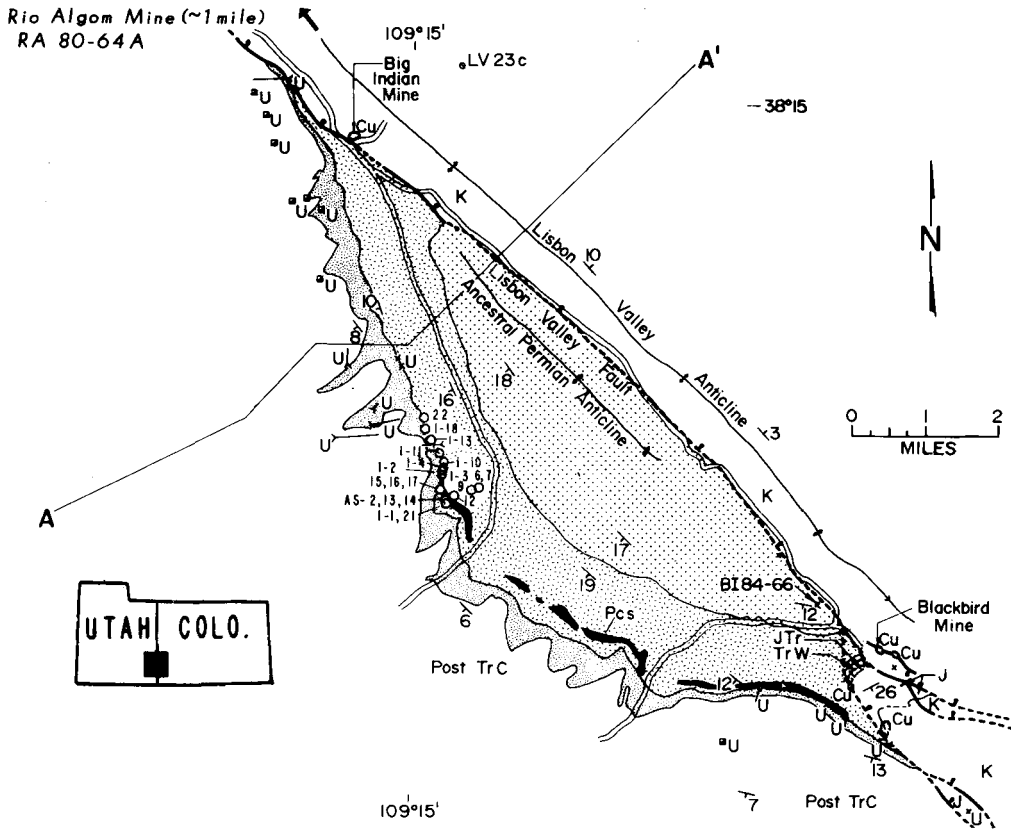
METHODS

Sample material for this study comes from well-exposed outcrops along Big Indian Valley (in the Lisbon Valley area), underground mine workings at the Rio Algom mine, and drill cores provided by Gulf Mineral Resources. Sample locations are shown on Figure 1.

Samples for X-ray powder diffraction (XRD) analyses were gently crushed and disaggregated in a blender with a small quantity of Calgon. The <2- μm size fraction was separated by centrifugation and treated with NaOAc buffered at pH 5 to remove carbonates. Red clays were treated with citrate-bicarbonate-dithionite (CBD) at 90°C to remove hematite and noncrystalline iron oxides prior to analysis (Jackson, 1969). The <2- μm fraction of sample BI-9 was pink due to residual iron oxide, but was not treated with CBD. The resulting suspensions were either sedimented on glass slides or filtered through 0.4- μm -pore-size silver membranes to produce oriented samples for XRD. Samples sedimented on glass slides appeared to be nearly pure corrensite, but were observed to contain a significant proportion of regularly interstratified illite/smectite (I/S)

Figure 1. (Upper) Geologic map, and (lower) cross section showing sample locations for the Lisbon Valley salt anticline. Geology after Wood (1968) from U.S. Geol. Survey Misc. Map series MF-124, MF-143, MF-145, and MF-147 through 151. Cross section after Parker (1968).





- | | | |
|----------------------|--|--|
| CRETACEOUS | | Contact (dashed where covered) |
| K | Mancos Sh, Dakota SS and Burro Canyon Fm. | |
| JURASSIC | | Fault (dashed where covered) |
| J | Morrison, Summerville, Entrada and Carmel Fms. | |
| JUR-TRIAS | | Anticline showing trace of axial plane and direction of plunge of axis |
| JTr | Navajo SS and Kayenta Fm. | |
| TRIASSIC | | Strike and Dip of Beds |
| TrW | Wingate SS | |
| TrC | Chinle Fm. | Drill Hole |
| PERMIAN | | |
| Pc | Cutler Fm. Pcs Sugar SS. | Road |
| PENNSYLVANIAN | | |
| Ph | Honaker Trail Limestone | Sample number prefixed by BI unless shown otherwise |
| | | |
| | | SHAFT |
| | | |
| | | ADIT |
| | | |
| | | OPEN PIT |
| | | |
| | | PROSPECT |
| | | |
- U = Uranium
Cu = Copper

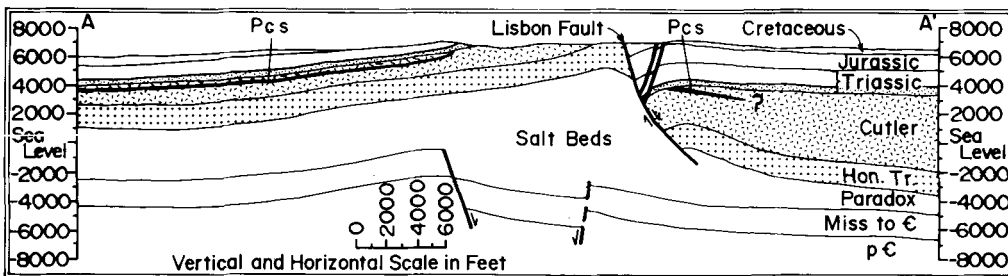


Table 1. Modal analyses of authigenic phases in selected Cutler samples, Lisbon Valley, Utah.

| Sample | Rock type ² | Grain size ³ | Clay ⁴ (%) | Clay ⁵ types | Cement ⁶ (%) | Cement types ⁷ |
|-----------------------------|------------------------|-------------------------|-----------------------|-------------------------|-------------------------|-----------------------------|
| Marine/eolian facies | | | | | | |
| BI-9 | quartz arenite | F | 1.4 | C/S | 21.5 | calcite |
| BI-1-4 | quartz arenite | VF | 4.2 | C/S | 20.4 | calcite |
| BI-1-3 | subarkose | F | 1.1 | C/S | 22.3 | calcite |
| BI-1-2 | quartz arenite | VF | 1.4 | C/S | 10.8 | calcite |
| BI-1-10 | subarkose | VF | 5.5 | C/S, I/S | 17.9 | calcite, barite |
| LV23C-2.0 | quartz siltstone | SLT | 14.1 | I, C, I/S | 36.0 | iron oxides, dolomite |
| Fluvial facies | | | | | | |
| BI-12 | arkose | M | 14.6 | I/S, C/S | 15.1 | calcite, iron oxides |
| RA-80-64A | arkosic wacke | F | 20.0 | S | 12.0 | carbonates |
| AS-2 | litharenite | C | 13.3 | S | 9.0 | iron oxide, calcite, quartz |
| BI-21 | subarkose | F | 8.8 | S | 29.7 | iron oxides |
| BI-14 | subarkose | F | 7.2 | n.d. | 2.6 | iron oxides |
| BI-22 | litharenite | C | <1.0 | S | 17.2 | calcite |
| BI-16 | siltstone | SLT | 1.9 | S, I | 51.3 | iron oxides, calcite |

¹ Based on about 500 point counts per thin section.

² Based on classification by Pettijohn *et al.*, 1973.

³ Predominant grain size based on approximately 200 counts. Grain size: SLT = silt, VF = very fine, F = fine, M = medium, C = coarse.

⁴ Modal percentage of clay in thin section.

⁵ Major clays listed in order of abundance. Clays listed comprise >80% of the <2- μ m fraction. C = chlorite, C/S = corrensite, I = illite, I/S = regularly interstratified illite/smectite, S = smectite. n.d. = not determined.

⁶ Modal percentage of cement in thin section.

⁷ Cement types listed in order of abundance.

when sedimented on filters. Unoriented XRD mounts were prepared by side-loading clay powders in aluminum holders. XRD analyses were made on a Philips XRD unit operated at 40 kV and 20 mA, at a scanning rate of 1°2 θ /min using a Cu target and a graphite monochromator.

Identifications of mixed-layer clays were based on Reynolds (1980), and simulated XRD profiles were computed using procedures of Reynolds (1980, 1983). To aid in mixed-layer clay identification, XRD patterns were made after four treatments: air drying at room temperature, glycolation for 24 hr, heating to 250°C for 1 hr, and heating to 550°C for 1 hr.

The intensities of selected XRD peaks were measured for a semiquantitative estimate of the proportions of clay minerals present in the <2- μ m size fractions. Mineral percentages were calculated by multiplying an estimated weighting factor by the peak intensity and then normalizing to 100%:

$$i\% = 100(\text{MIF}_i)(I_i)/(\sum_j(\text{MIF}_j)(I_j)),$$

where $i\%$ = weight percent of clay mineral i in sample, MIF_i = mineral intensity factor for i from Table 2, I_i = measured intensity of i (peak area), and \sum_j = summation of all clays. MIFs were estimated using ratios of absolute peak areas from calculated XRD profiles of pure clays (Reynolds, 1980, 1983), and intensities were calculated by measuring areas under peaks. Inaccuracies of estimated clay abundances resulted from the inability to differentiate overlapping peaks, and

differences in X-ray absorption due to variable thicknesses and chemical compositions. This procedure is probably accurate to $\pm 10\%$ of the amount present.

Splits of selected clay samples used for XRD were analyzed for major elements by atomic absorption (AA). Samples were fused with Li-metaborate for 1.5 hr over gas-compressed air flame and dissolved in dilute HCl.

Thin sections were stained with alizarin-red S and potassium ferricyanide to distinguish various types of carbonate cements. Twenty-one thin sections of Cutler samples were examined for mineral and textural relationships and 13 were point counted. Sandstones were classified based on petrography.

RESULTS

Petrography

Marine and eolian sandstones are typically only slightly feldspathic, ranging from quartz arenite to subarkose, whereas fluvial sandstones contain abundant K-feldspar, plagioclase, and igneous and metamorphic rock fragments.

The clay content of the marine and eolian sandstones examined here is commonly low, and the rocks contain corrensite as the dominant clay mineral, together with lesser amounts of regularly interstratified I/S and minor illite and chlorite (Tables 1 and 2). The fluvial facies contains predominantly smectite in the <2- μ m size fraction and minor chlorite and illite. Corrensite forms thin rims on detrital grains barely visible in thin

Table 2. Estimated proportion of clay minerals in <2- μ m size fractions (%).¹

| Sample | C/S | I | S | I/S | C |
|--------------------------|-----|----|-----|-----|----|
| Marine-eolian sandstones | | | | | |
| BI-9 ² | 92 | 8 | 0 | 0 | tr |
| BI-1-4 ² | 84 | 6 | 0 | 10 | 0 |
| BI-1-13 ² | 75 | 0 | 0 | 25 | 0 |
| BI-1-18 ² | 86 | 0 | 0 | 14 | 0 |
| BI-1-2 | 95 | 5 | 0 | tr | 0 |
| BI-1-3 | 87 | 0 | 0 | 13 | 0 |
| BI-6 | 91 | 9 | 0 | 0 | 0 |
| LV23C-9.4 ² | 0 | 13 | 82 | 0 | 5 |
| BI-1-10 | 60 | 0 | 0 | 40 | 0 |
| LV23C-2.0 | 0 | 38 | 0 | 25 | 37 |
| BI-1-1 | 32 | 0 | 68 | 0 | 0 |
| BI-1-11 | 62 | 0 | 0 | 38 | 0 |
| Fluvial sandstones | | | | | |
| RA-80-64A | 0 | 0 | 100 | 0 | 0 |
| AS-2 | 0 | 0 | 100 | 0 | tr |
| BI-14 | 96 | 4 | 0 | 0 | 0 |
| BI-21 | 0 | 3 | 97 | 0 | 0 |
| BI-12 | 38 | 0 | 0 | 62 | 0 |
| BI-15 ² | 96 | 3 | 0 | 0 | 1 |
| BI-22 ² | tr | 0 | 100 | 0 | 0 |
| Shales/siltstones | | | | | |
| BI-16 ² | 0 | 16 | 75 | 0 | 9 |
| BI-17 | 0 | 73 | 4 | 0 | 23 |
| BI-13 | 98 | 2 | 0 | tr | 0 |
| Limestone | | | | | |
| BI-84-66 | 89 | 11 | 0 | 0 | 0 |

¹ Estimates made using the following mineral intensity factors (MIF) determined by ratios of the pure mineral peaks from calculated diffraction profiles using Reynolds' (1980, 1983) Mod-8 computer program: illite 001 = 1.0, corrensite 006 = 2.9, smectite 003 = 2.6, chlorite 003 = 1.4, and regularly interstratified I/S 003 (~60% I) = 2.5. C = chlorite, C/S = corrensite, I = illite, I/S = regularly interstratified illite/smectite, S = smectite, tr <1%.

² Sample used for atomic absorption analyses.

section, but smectite forms thick rims and commonly fills pore space. Sandstones containing smectite as the dominant clay mineral usually contain a higher proportion of clay (as much as 20%) than those dominated by corrensite; smectite is therefore more abundant than corrensite in the Cutler stratigraphic section.

Fe-poor (determined by staining) calcite cement is the dominant non-clay cement present and comprises about 20% of the marine and eolian sandstones. Nearly all the detrital minerals have been partially replaced by calcite. Sparry calcite cement appears to have invaded at grain boundaries and to have occluded former pore spaces. Grains are commonly completely replaced by calcite. Grain boundaries preserved as iron oxide shadows enclosed by calcite remain, providing evidence that prior to calcite replacement, framework grains were more abundant. Barite cement comprises 4.5% of the total cement in one sample (BI-1-10) of eolian sandstone. Barite cements are also present in

several samples of the basal Chinle Formation (Moss Back Member), comprising as much as 20% of one sample. Barium is also concentrated in Cutler uranium ore zones (Campbell and Steele-Mallory, 1979) and may have been introduced by ore-forming fluids.

Hematite is commonly the most abundant cement in the smectite-rich sandstones. Quartz overgrowths are rare, but may have been more abundant prior to calcite cementation. Fe-rich dolomite cement although common to the overlying Moss Back was not found in Cutler samples. Fe-poor dolomite was found in only one sample (LV 23C-2.0), where it made up 100% of the cement.

Individual feldspar grains commonly display variable degrees of argillic alteration ranging from almost unaltered to complete replacement within the same thin section. Light dustings of sericite are most common. No authigenic feldspar was observed. A few individual sand grains are partially or completely chloritized, and foliated (schistose) textures were commonly observed. No detrital pyroxenes, amphiboles, or iron-titanium oxide grains were observed. Accessory minerals include garnet, tourmaline, apatite, and zircon. Detrital micas commonly make up 1–2% of the quartz arenites and arkoses, and as much as 20% of the red siltstones. Detrital micas are relatively unaltered, except for invasion by calcite cements. Rock fragments are rare in the marine and eolian arenites, but are common in the fluvial arkoses. Most rock fragments are polycrystalline quartz, or quartz and feldspar, indicating a granitic or gneissic source.

Clay mineral distribution

XRD profiles of glycolated samples used for chemical analysis and of simulated regularly interstratified I/S and corrensite are shown in Figure 2. Most corrensites displayed a prominent chlorite + (ethylene glycol) smectite 001 superlattice reflection at 31 Å (2.8°2 θ). Regular short-range ordering was indicated by a series of peaks at positions corresponding to integral reflections of the superlattice corrensite 001 peak. Sharp peaks were common through 00,11, the upper limit of the runs. At low values of 2 θ , even-order peaks were strongest, whereas at high angles, odd-order peaks were most intense. All patterns showed strong basal reflections at n = 1, 2, 4, 6, 7, 9, and 11, but intervening peaks were weak or absent. The patterns showed good agreement with the simulated profile for dioctahedral corrensite. Regular integral d-values, sharp superlattice reflections, and the positions of the 004 reflection of glycolated corrensite near 7.8 Å and the 009 reflection of glycolated corrensite near 3.45 Å (Table 3) suggest nearly a 1:1 ratio of chlorite to smectite layers. Small variations in the positions of the 004 and 009 peaks coinciding with decreasing intensity of the superlattice

001 peak, indicate as much as a few percent deviation from ideal 1:1 composition in some samples.

Regularly interstratified I/S was indicated by the presence of broad superlattice 002 peak at about 13.6 Å in glycolated samples. The superlattice I/S 001 peak was rarely present. Ordered interstratification of the alleverdite type was demonstrated by the occurrence of a regularly interstratified I/S 002 peak and nearly regular, integral, high-angle reflections. Reflections near 9.2 and 5.3 Å (Table 3) indicate the presence of about 60% illite layers in I/S. The XRD pattern of analyzed regularly interstratified I/S was similar to the simulated pattern (Table 3). Glycolated smectites showed strong 001 reflections near 17 Å. The 003 peak was present but weak, and most other peaks of smectite were weak or absent.

Random powder mounts of selected samples were analyzed by XRD to determine the degree of contamination and to determine the d-value of 060 for subgroup designation (Table 4). Corrensite-rich samples showed two closely spaced peaks near 1.502 and 1.507 Å, both of which are consistent with dioctahedral site occupancy. No peaks were observed in the range 1.52–1.57 Å of trioctahedral phyllosilicates. It is not certain which peak corresponds to chlorite or to smectite layers nor could the extent of interference by regularly interstratified I/S in the sample be determined. Different specimens show consistent 060 peak positions and intensity regardless of small amounts of regularly interstratified I/S contamination, suggesting that 060 reflections due to regularly interstratified I/S are minor.

Estimated clay mineral abundances are listed in Table 2. Corrensite was found to be more abundant in the marine and eolian arenites, whereas smectite dominated in the fluvial arkoses. Insoluble residue from a single sample (BI-84-66) of Hermosa limestone adjacent to the Lisbon Valley fault contained substantial amounts of corrensite that was poorly ordered compared with those from sandstones, as indicated by lack of a superlattice 001 peak and presence of a broad 002 peak. Two samples from Cutler uranium mines in Spillar Canyon (AS-2) and the Standard Big Buck mine (BI-22) are oxidized igneous litharenites, and contain smectite as the most abundant clay mineral.

Clay mineral geochemistry

Samples having minimal contamination were selected for chemical analyses by atomic absorption spectrometry. Corrensite-dominated specimens contained small amounts of regularly interstratified I/S. The ratio of corrensite to I/S indicated by the XRD intensity ratios of the 008 peak of glycolated I/S to the 009 peak of corrensite are plotted against weight percent MgO, Fe₂O₃, Al₂O₃, and SiO₂ (Table 5) in Figure 3. The XRD peaks used were well defined on all patterns and had similar d-values so that errors related to variation of

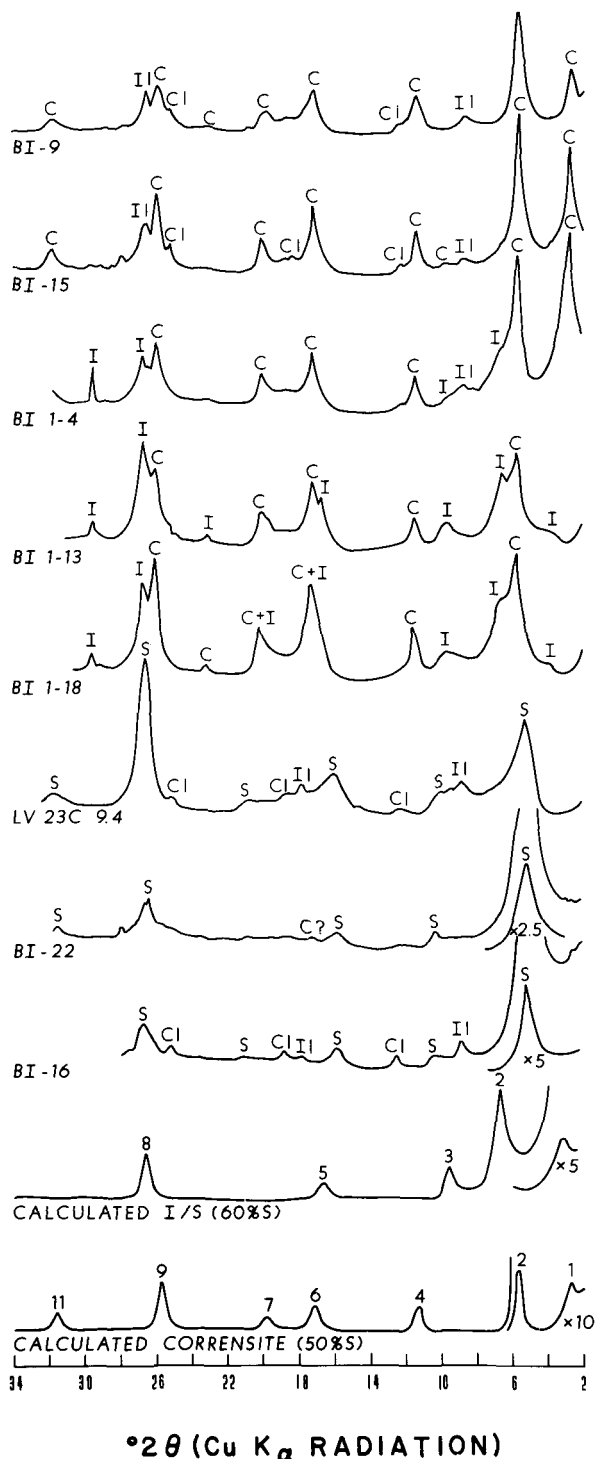


Figure 2. X-ray powder diffraction patterns of oriented, glycolated samples used for chemical analyses. The bottom two are simulated patterns of dioctahedral corrensite and regularly interstratified illite/smectite (60% illite layers). Numbers indicate the order of the basal reflection. C = corrensite, I = regularly interstratified I/S, S = smectite, Cl = chlorite, Il = illite. Abscissa = 2θ , CuK α radiation.

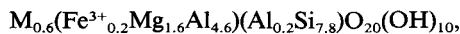
Table 3. X-ray powder diffraction peaks (Å) for corrensite and illite/smectite clays from selected samples and computed synthetic patterns.

| | BI-9 | | | BI-1-11 | | | Syn C/S | Syn I/S |
|----------|-------------|-------------|-------------|-------------|-------------|------------|-------------|-------------|
| | A.D. | Gly | 550°C | A.D. | Gly | 550°C | Gly | Gly |
| C/S 001 | 29.95 (29) | 32.13 (22) | 26.66 (15) | 27.18 (100) | 30.46 (100) | | 31.55 (45) | |
| I/S 001 | | | | | 28.05 (6) | | | 27.61 (100) |
| C/S 002 | 14.42 (100) | 15.50 (100) | 11.87 (100) | 13.60 (31) | 15.24 (11) | 11.63 (6) | 15.50 (100) | |
| I/S 002 | | | | 11.48 (75) | 13.60 (21) | | | 13.39 (70) |
| I 001 | 10.05 (2) | 10.16 (9) | 10.06 (13) | | | 9.94 (100) | | |
| C/S 003 | 9.56 (11) | | | 9.03 (5) | | 7.97 (2) | | |
| C/S 004 | 7.17 (12) | 7.75 (26) | | 7.25 (3) | 7.69 (2) | | 7.80 (13) | |
| C/S 005 | 5.62 (2) | | | 5.34B (7) | | | | |
| I/S 003 | | | | | 9.21 (4) | | | 9.21 (17) |
| I/S 005 | | | | | 5.37 (4) | | | 5.34 (9) |
| C/S 006 | 4.74 (57) | 5.16 (38) | | | 5.22 (5) | | 5.15 (12) | |
| C/S 007 | | 4.46 (10) | | | | | 4.46 (6) | |
| C/S 008 | 3.55 (32) | | | 3.31B (2) | | | | |
| I/S 007 | | | | 3.24 (15) | | | | |
| I/S 008 | | | | | | | | 3.35 (28) |
| I 003 | 3.35 (8) | 3.35 (8) | | | | | | |
| C/S 009 | 3.20 (1) | 3.43 (19) | | | | | 3.47 (19) | |
| C/S 0010 | 2.84 (8) | | | | | | | |
| C/S 0011 | 2.62 (<1) | 2.82 (11) | | | | | 2.83 (6) | |

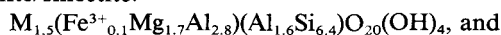
A.D. = air dried, Gly = glycolated, C/S = corrensite, I/S = illite/smectite, I = illite, 550°C = heated at 550°C. Relative intensity in parentheses. BI-9 and BI-1-11 are sample numbers. Syn indicates patterns computed from the Mod-8 program (Reynolds, 1980, 1983).

the angle of the incident X-ray beam were minimal. The intersections of best fit lines for each data set with the horizontal axis ($I/S = 0$) determined the weight percent oxide in the corrensite. A similar procedure using the inverse ratio (corrensite 009/I/S 008) was used to determine the weight percents of oxides in I/S. Exchangeable cation oxides (CaO , Na_2O , and K_2O) plotted in a similar manner showed significant scatter, suggesting that cation exchange took place prior to and/or during treatment for analysis. The following structural formulae were calculated from oxide weight percents in Figure 3 for regularly interstratified I/S and corrensite and using sample BI-22 (Table 5) to represent an average smectite:

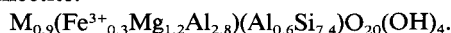
corrensite:



illite/smectite:



smectite:



Layer charges of 0.60, 1.50, and 0.90, respectively, for corrensite, I/S, and smectite (satisfied by undesignated monovalent cation (M)) were used. The oxidation state of Fe was not determined because the total Fe content was low and was assumed to be 3+.

Lisbon Valley corrensite is highly aluminous having 6.4 of 9 possible octahedral sites (6 sites in chlorite and 3 sites in smectite) filled, supporting the di/dioctahedral nature determined by XRD methods. About 75% of the filled octahedral sites are occupied by Al,

and the remaining 25% by Mg. Fe is a minor component, making up about 3% of the octahedral sites. Most of the corrensites tabulated in Brigatti and Poppi (1984) have excess layer charge indicating that some K may be fixed in interlayer brucite or gibbsite sheets. Corrensites from the present study and those listed by Brigatti and Poppi (1984) are plotted on triangular composition diagrams in Figure 4. Lisbon Valley corrensite plots near other di/dioctahedral corrensites, but it is lower in Fe and richer in Al. Fields of trioctahedral vs. dioctahedral corrensites are well defined, and the chemical similarities between the Lisbon Valley corrensite, regularly interstratified I/S, and smectite are apparent.

The smectites appear to be dioctahedral, as shown by 060 spacings (Table 4) and octahedral site occupancies of 4.1 to 4.3 (of 6 available sites) from chemical analysis. Except for sample LV23C-9.4, layer charges

Table 4. $d(060)$ values of selected samples.

| Sample | $d(060)$ value (Å) | Clay types |
|----------|-----------------------|------------|
| BI-15 | 1.501/1.506 (doublet) | C/S + I/S |
| BI-1-13 | 1.502/1.506 (doublet) | C/S + I/S |
| BI-1-4 | 1.505/1.508 (doublet) | C/S + I/S |
| BI-6 | 1.507 | C/S |
| BI-22 | 1.501 | S |
| LV23C9.4 | 1.501 | S |

C/S = corrensite, I/S = regularly interstratified illite/smectite, S = smectite.

Table 5. Uncorrected oxide weight percentages for clay minerals determined by atomic absorption.¹

| Sample | SiO ₂ | Al ₂ O ₃ | MgO | Fe ₂ O ₃ ² | Na ₂ O | K ₂ O | CaO |
|-------------------------------------|------------------|--------------------------------|------|---|-------------------|------------------|-----|
| Corrensite-dominated samples | | | | | | | |
| BI-9 | 53.9 | 27.1 | 11.7 | 5.3 | 1.0 | 0.4 | 0.5 |
| BI-15 | 54.9 | 31.2 | 7.3 | 2.0 | 1.5 | 2.6 | 0.4 |
| BI-1-4 | 55.8 | 28.6 | 7.5 | 1.9 | 0.0 | 3.7 | 2.5 |
| BI-1-13 | 54.1 | 31.2 | 9.2 | 1.2 | 1.1 | 2.3 | 0.9 |
| BI-1-18 | 53.9 | 29.8 | 8.7 | 1.7 | 0.3 | 4.3 | 1.4 |
| Smectite-dominated samples | | | | | | | |
| LV23C-9.4 | 58.4 | 26.8 | 5.4 | 2.5 | 2.0 | 4.9 | 0.0 |
| BI-22 | 62.1 | 23.8 | 6.8 | 3.5 | 3.1 | 0.8 | 0.0 |
| BI-16 | 60.9 | 25.2 | 5.7 | 3.2 | 2.6 | 2.0 | 0.2 |

¹ Calculated on a water-free basis.

² Total Fe calculated as Fe₂O₃.

are within an ideal range (0.6 to 1.0) for smectites based on the O₂₀(OH)₄ structural unit. The high layer charge of sample LV23C-9.4 is probably due to an erroneously high K₂O analysis. About two-thirds of the filled octahedral sites are occupied by Al, and the rest by Mg. Smectites from this study are chemically similar to di/dioctahedral corrensites, as indicated by the composition of BI-22 (open square) on Figure 4.

DISCUSSION

The three stages of authigenic mineral precipitation recognized in Cutler sandstones in the Lisbon Valley area are: (1) quartz overgrowths, (2) smectite and corrensite, and (3) calcite. Iron oxide occurs as either a pervasive diffuse stain throughout the cement and matrix or as opaque disseminations and grain coatings. At least some iron oxide precipitated early as shown by hematite rims on quartz grains that were then coated by quartz overgrowths. The precipitation of quartz as

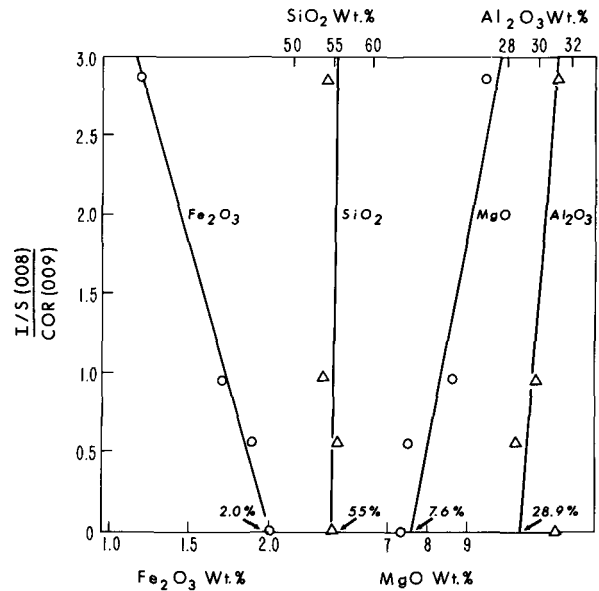


Figure 3. Oxide weight percentages vs. relative abundances of illite/smectite to corrensite XRD peak ratios. Best fit lines intersect abscissa at oxide weight percent in corrensite. Sample BI-9 contained significant Fe-oxide contamination and was omitted from diagram. Circles are Fe₂O₃ or MgO; triangles are SiO₂ or Al₂O₃.

grain overgrowths was followed by authigenic clay minerals. The dominance of smectite in impermeable, fluvial, red-bed arkoses and its relative absence in more permeable marine and eolian arenites suggests that early-formed smectite was removed or transformed to corrensite by fluids migrating through the permeable rock units. The third stage of mineral formation involved a massive influx of Fe-poor carbonate cements

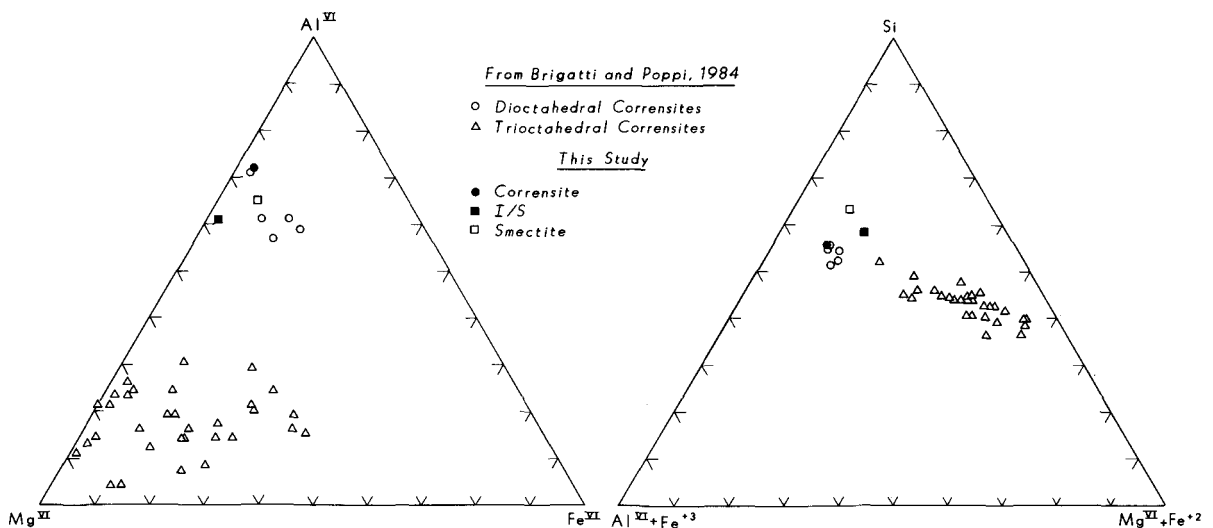


Figure 4. Triangular plots of (a) octahedral cation site occupancy and (b) Si vs. octahedral trivalent and octahedral divalent cations.

Table 6. Summary of thermodynamic properties of corrensite, illite/smectite, and smectite.

| Mineral | | Structural formula | | | | | | |
|----------|------------------|---|---|---|---|-----------------|--------------------|--|
| C/S | | $K_{0.70}(Mg_{1.65}Al_{4.74})(Al_{0.20}Si_{7.80})O_{20}(OH)_{10}$ | | | | | | |
| I/S | | $K_{1.50}(Mg_{1.70}Al_{2.90})(Al_{1.60}Si_{6.40})O_{20}(OH)_4$ | | | | | | |
| Smectite | | $K_{0.70}(Mg_{1.65}Al_{2.87})(Al_{0.60}Si_{7.40})O_{20}(OH)_4$ | | | | | | |
| Mineral | ΔG° | ΔH° | S | V | a | $b \times 10^3$ | $c \times 10^{-5}$ | |

Properties at 298°C

| | | | | | | | |
|----------|-------------|-------------|--------|--------|---------|--------|--------|
| C/S | -13,137,489 | -14,148,222 | 720.92 | 344.15 | 1030.58 | 317.81 | 260.96 |
| I/S | -11,178,197 | -11,937,494 | 571.57 | 280.67 | 746.76 | 314.00 | 177.23 |
| Smectite | -10,865,784 | -11,613,766 | 544.95 | 270.19 | 848.46 | 97.81 | 216.98 |

ΔG , ΔH in joules/mole; S in joules/K/mole; V in cm^3 /mole; a, b, c are coefficients for the heat capacity equation: $C_p = a + bT - cT^{-2}$ where C_p in joules/K/mole. C/S = corrensite, I/S = illite/smectite.

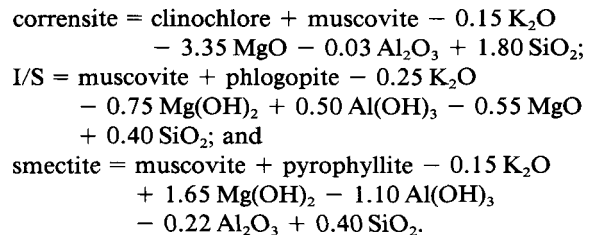
which corroded or destroyed much of the framework of detrital grains.

Smectite is volumetrically the most important authigenic clay phase in the Cutler section in the Lisbon Valley area and is now abundant in low-permeability arkosic sandstones and siltstones. It is typically the sole clay mineral in these samples, except for minor amounts of chlorite and illite, and, in one sample, corrensite. Corrensite is typically present in permeable eolian and marine sandstones. The distribution of corrensite and smectite suggests that the formation of the clay minerals was controlled by pore-fluid chemistry. Both smectite and corrensite may have formed from the same fluid that chemically evolved by the interaction with the host rock, or each clay may have formed from separate generations of fluid migration. Clay minerals could have formed during Permian weathering, burial diagenesis, or Recent weathering. The available fluids include Permian surface water, seawater, formation fluids (evolved meteoric or connate fluids), and Recent meteoric water. Analogous clay assemblages from drill cores and mine workings at a depth of 860 m precludes the third possibility of Recent weathering.

Corrensite is commonly found in hypersaline deposits with limestones, suggesting a chemical control on its genesis (Grim *et al.*, 1960; Kopp and Fallis, 1974; Weaver *et al.*, 1982). Occurrences in hydrothermal environments, contact metamorphosed shales, and increasing abundance at depth during burial diagenesis suggests that temperature has a significant effect either on mineral stability or on kinetics of formation. Precise equilibrium assessment of intensive variables (cation chemical potentials, temperature, and pH) is limited by the lack of thermodynamic data for corrensites.

Logarithmic activity diagrams were constructed using free energy estimates for mixed-layer clays computed by the method of Tardy and Garrels (1974). Free energies of clay minerals were estimated by summing the calculated free energies of oxide components associated with silicate octahedral sites, silicate tetrahedral sites, and exchangeable sites. This procedure makes no allowance for mixed-layering, thus a corrensite was assigned a free energy value identical to that

assigned to a mixture of discrete chlorite and smectite with the same composition. Thermodynamic data for corrensite, I/S, and smectite used in the phase equilibria analysis that follows are given in Table 6. Structural formulae for these clays as computed above were adjusted slightly so that Fe was eliminated and interlayer cation sites were filled by K. Enthalpy, entropy, molar volume, and heat capacity were estimated by combinations of C_p , H, S, and V data on minerals and oxides from Helgeson *et al.* (1978) as follows:



Similar results were obtained from summation of parameters of mineral constituent oxides. Equilibrium constants at elevated temperatures and pressures were then calculated using the computer algorithm SUPCRT (Helgeson *et al.*, 1978) to integrate the heat capacity expressions.

Equilibrium among clay minerals and aqueous solutions at temperatures of 25° and 100°C is portrayed on the equilibrium activity diagrams shown in Figure 5. Figure 5a shows relationships at 25°C and 1 bar pressure with dissolved silica activity fixed at solid noncrystalline silica saturation. Figure 5b shows mineral stability fields at 100°C and 300 bar pressure and dissolved silica fixed at quartz saturation (solid lines) or noncrystalline silica saturation (dashed lines). Five Paradox basin formation waters of variable ionic strengths from McCulley *et al.* (1984) are plotted on the diagrams along with seawater activity ratios calculated by Garrels and Thompson (1962). Activities were determined using the computer program WATEQ (Truesdell and Jones, 1974). Activity ratios using laboratory determined pH measurements are shown as circles, and triangles represent activity ratios at one lower pH unit.

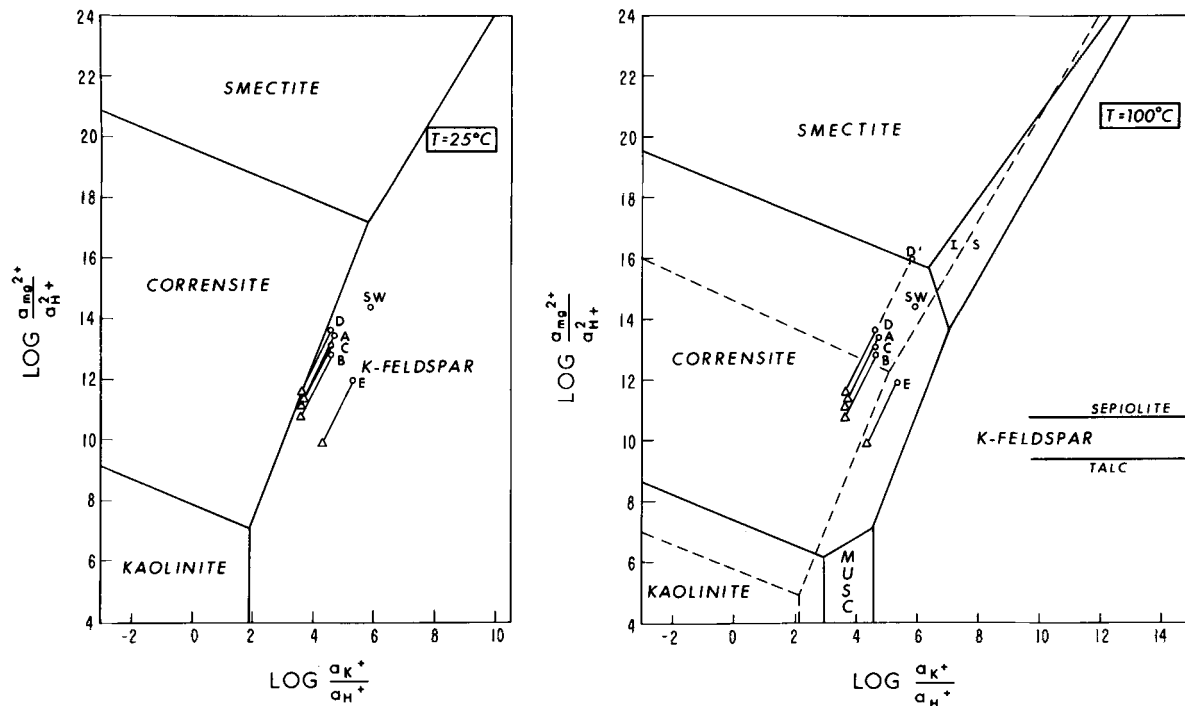


Figure 5. Activity diagrams for the system $K_2O-MgO-Al_2O_3-SiO_2-H_2O$. Al is conserved among solid phases. (a) $T = 25^\circ C$, $P = 1$ bar, noncrystalline silica saturation. (b) $T = 100^\circ C$, $P = 300$ bars, solid and dashed lines indicate quartz and noncrystalline silica saturation, respectively. $\text{Log}(a_{Mg^{2+}}/a_{H^+}^2)$ values for sepiolite (+ quartz) and talc (+ quartz) saturations are shown for reference.

Formation fluids from the Gibson dome borehole (McCulley *et al.*, 1984) as follows:

| | Sample | Rock unit | Ionic strength | Lab. pH |
|---|-----------|------------------------|----------------|---------|
| A | GW-028-01 | Cutler/Elephant Canyon | 0.16 | 8.3 |
| B | GW-033-01 | Honaker Trail | 2.47 | 7.1 |
| C | GW-029-01 | Cutler/Honaker Trail | 0.10 | 8.3 |
| D | GW-032-01 | Elephant Canyon | 0.24 | 8.2 |
| E | GW-041-01 | Leadville | 1.49 | 7.0 |

SW = seawater. Circles represent fluids calculated at laboratory-determined pH. Triangles are calculated at 1 pH unit lower than laboratory pH. Path DD' is discussed in text.

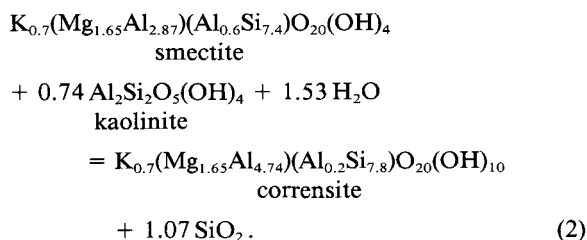
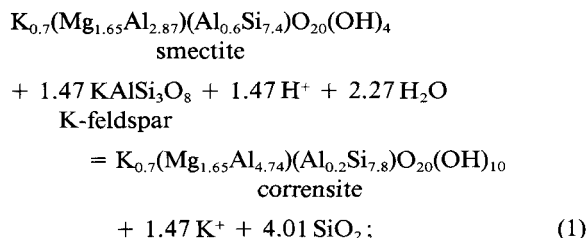
Natural waters fall within the K-feldspar stability field near equilibrium with corrensite at $25^\circ C$ (Figure 5a), but at $100^\circ C$, the waters are within the corrensite (plus quartz) field (Figure 5b, solid lines). At higher dissolved silica values (noncrystalline silica saturation), I/S and muscovite are metastable, and most plotted waters fall in the smectite stability field at laboratory-determined pH, but in the corrensite field for more acidic waters. Thus, smectite will form from alkaline solutions at temperatures approaching $100^\circ C$ at high silica concentrations. If dissolved silica concentration falls to quartz saturation, these same fluids will precipitate corrensite. Most current formation fluids in Permo-Pennsylvanian rocks of the Paradox basin are slightly undersaturated with respect to noncrystalline silica, but oversaturated with respect to quartz at surface temperatures (data from McCulley *et al.*, 1984;

Hanshaw and Hill, 1969). Quartz overgrowths present in the Cutler sugar sandstones indicate at least one stage of quartz precipitation, and locally corrensite was observed overgrown on (i.e., later than) quartz overgrowths.

Fe-rich chlorite has been experimentally transformed to smectite via intermediary corrensite by subjecting it to strongly oxidizing conditions simulating weathering, and the rate of reaction was increased by high Fe concentrations and with more Fe distributed in the interlayer hydroxide sheets (Senkayi *et al.*, 1981). These experiments suggest that corrensite may form from precursor smectite by reduction of iron. The low Fe content of the Lisbon Valley corrensite and smectite precludes such oxidation-reduction transformations. Chlorite (clinochlore) is stable with respect to corrensite over the entire range of Figure 5, and, upon deeper

sediment burial accompanied by enhancement of chlorite precipitation kinetics, corrensite should transform to chlorite.

The formation of corrensite from precursor smectite may be a mole-for-mole conversion with the addition of Al. Two Al-conservation reactions are proposed, with kaolinite or K-feldspar as a source of Al:



Mg is conserved between smectite and corrensite in both reactions and Al is conserved among solids.

If corrensite forms from smectite via reaction (1), H^+ is consumed and K^+ is produced. In a closed system such as might exist if pore water is buried in a shaly, impermeable rock unit, fluid composition will evolve as the fluid approaches equilibrium with reactive phases in the rock. For example, fluid D (Figure 5b) will change composition along path DD' as smectite + K-feldspar are converted to corrensite + quartz. The pore fluid will remain at point D' in equilibrium with the rock. Less than 1% of the smectite would be converted to corrensite during the evolution of fluid chemistry to point D', and such a small amount would not be detectable by standard XRD procedures. If the pore fluid is maintained at point D under open-system conditions, corrensite would continue to form until all the smectite was consumed. For complete conversion of 10 volume percent smectite to corrensite by maintaining incoming solution composition between points D and D' without external pH buffering, an unreasonably large fluid flow would be required ($\sim 10 \times 10^6$ pore volumes; assuming 30% porosity and an initial pH of 8.2). If the solution is externally buffered at constant pH (pH = 8.2 in this calculation), by for example, CO_2/CH_4 or $\text{H}_2\text{S}/\text{SO}_4^{2-}$ equilibria, only about two pore-fluid volumes are required to convert all the smectite to corrensite.

Aluminous corrensite should have formed from smectite in contact with basin fluids under conditions of elevated temperature and decreased silica activity, as the solutions change in composition from noncrystalline silica to quartz saturation.

Smectite probably formed from solutions at higher pH, whereas corrensite was stable under more acid conditions. I/S was stable only under conditions of reduced silica concentration. At dissolved SiO_2 values between quartz and noncrystalline silica saturation, such as are common in Paradox basin fluids, I/S and corrensite probably formed a stable assemblage in equilibrium with pore fluid (compare the quartz- and noncrystalline silica-saturated diagrams in Figure 5b). Mole-for-mole conversion of smectite to corrensite must have been accompanied by Al addition from solution.

Reaction (2) allows a molar conversion of smectite to corrensite with release of silica to solution and the conservation of both Mg and K among the solids. Computed ΔG s for reaction (2) are less than -6.5 kcal/mole for all values of T from 25° to 120°C at quartz- and noncrystalline silica-saturation, indicating that corrensite is the stable phase with respect to smectite + kaolinite under all natural dissolved-silica concentrations.

Corrensite may have formed at any time after deposition of the sediment. Elevated temperature ($\sim 100^\circ\text{C}$) favors corrensite, suggesting either that it formed at burial depths of 3–4 km, or the presence of a local thermal anomaly. Calcite-sulfide veins along the Lisbon Valley fault crystallized at $\sim 100^\circ\text{C}$, based on fluid-inclusion homogenization temperatures (Morrison and Parry, 1986). These thermal fluids migrating up along the fault could have permeated Cutler sandstones and caused the phyllosilicate alterations. The similarity of the clay assemblages throughout the entire Cutler stratigraphic section and in the Hermosa limestone precludes any direct relationship of corrensite formation to uranium deposits in the overlying Chinle Formation.

ACKNOWLEDGMENTS

Funding was provided by fellowships from the University of Utah and the American Federation of Mineralogical Societies to S.J.M. and University of Utah Mineral Leasing Fund to W.T.P. Gulf Mineral Resources donated drill cores from Lisbon Valley. Thure Cerling provided helpful suggestions to improve the manuscript. Critical reviews by R. C. Reynolds and Y. Tardy greatly improved the manuscript.

REFERENCES

- April, R. H. (1980) Regularly interstratified chlorite/vermiculite in contact metamorphosed red beds, Newark Group, Connecticut Valley: *Clays & Clay Minerals* **28**, 1–11.
- Bailey, S. W. (1980) Summary of recommendations of AIPEA nomenclature committee on clay minerals: *Amer. Mineral.* **65**, 1–7.
- Blatter, C. L., Roberson, H. E., and Thompson, G. R. (1973) Regularly interstratified chlorite-dioctahedral smectite in dike-intruded shale, Montana: *Clays & Clay Minerals* **21**, 207–212.

- Bradley, W. F. and Weaver, C. E. (1956) Chlorite-vermiculite: *Amer. Mineral.* **41**, 497–504.
- Brigatti, M. F. and Poppi, L. (1984) Crystal chemistry of corrensite: A review: *Clays & Clay Minerals* **32**, 391–399.
- Campbell, J. A. and Steele-Mallory, B. A. (1979) Uranium in the Cutler Formation, Lisbon Valley, Utah: in *Perrinland, Guidebook to the 9th Field Conf.*, D. L. Baars, ed., Four Corners Geol. Soc., Durango, Colorado, 23–32.
- Earley, J. W., Brindley, G. W., McVeagh, W. J., and Vanden Heuvel, R. C. (1956) Montmorillonite-chlorite: *Amer. Mineral.* **41**, 258–267.
- Frank-Kamenetsky, V. A., Logvinenko, N. V., and Drits, V. A. (1963) Tosudite—A new mineral forming the mixed-layer phase in alushite: in *Proc. Int. Clay Conf., Stockholm, Sweden, 1963, Vol. 2, I. Th. Rosenqvist and P. Graff-Petersen*, eds., Pergamon Press, Oxford, 181–186.
- Furbish, W. J. (1975) Corrensite of deuteric origin: *Amer. Mineral.* **60**, 928–930.
- Garrels, R. M. and Thompson, M. E. (1962) A chemical model for sea water at 25°C and one atmosphere total pressure: *Amer. J. Science* **260**, 57–66.
- Grim, R. E., Droste, J. B., and Bradley, W. F. (1960) A mixed-layer clay mineral associated with an evaporite: in *Clays and Clay Minerals, Proc. 8th Natl. Conf., Norman, Oklahoma, 1959*, Ada Swineford, ed., Pergamon Press, New York, 228–236.
- Hanshaw, B. B. and Hill, G. A. (1969) Geochemistry and hydrodynamics of the Paradox basin region, Utah, Colorado, and New Mexico: *Chem. Geol.* **4**, 263–294.
- Helgeson, H. C., Delany, J. M., Nesbitt, H. W., and Bird, D. K. (1978) Summary and critique of the thermodynamic properties of rock-forming minerals: *Amer. J. Science* **278-A**, 1–229.
- Jackson, M. L. (1969) *Soil Chemical Analysis—Advanced Course*, 2nd ed., published by the author, Madison, Wisconsin, 895 pp.
- Johnson, L. J. (1964) Occurrence of regularly interstratified chlorite-vermiculite as a weathering product of chlorite in a soil: *Amer. Mineral.* **49**, 556–572.
- Kopp, O. C. and Fallis, S. M. (1974) Corrensite in the Wellington Formation, Lyons, Kansas: *Amer. Mineral.* **59**, 623–624.
- Kubler, B. (1973) La corrensite, indicateur possible de milieux de sédimentation et du degré de transformation d'un sédiment: *Bull. Centre Rech. Pau SNAP* **7**, 543–556.
- Lippman, F. (1954) Über einen Keuperton von Zaisersweiker bei Maulbronn: *Heidl. Beitr. Mineral. Petrog.* **4**, 130–134.
- Mack, G. H. and Rasmussen, K. A. (1984) Alluvial-fan sedimentation of the Cutler Formation (Permo-Pennsylvanian) near Gateway, Colorado: *Geol. Soc. Amer. Bull.* **95**, 109–116.
- McCulley, B. L., Thackston, J. W., and Preslo, L. M. (1984) Status report: Geochemical interactions between ground water and Paleozoic strata, Gibson dome area, southeastern Utah: Unnumbered BMI/ONWI topical report, prepared by Woodward-Clyde Consultants for Battelle Memorial Institute, Office of Nuclear Waste Isolation, Columbus, Ohio, 78 pp.
- Millot, G. and Camez, T. (1963) Genesis of vermiculite and mixed-layer vermiculite in the evolution of the soil of France: in *Clays and Clay Minerals, Proc. 10th Natl. Conf., Austin, Texas, 1961*, Ada Swineford and D. C. Franks, eds., Pergamon Press, New York, 90–95.
- Morrison, S. J. and Parry, W. T. (1986) Formation of carbonate-sulfate veins associated with copper ore deposits from saline basin brines, Lisbon Valley, Utah: Fluid inclusion and isotope evidence: *Econ. Geol.* **81** (in press).
- Pacquet, A. (1968) Analcime et argiles diagenétiques dans les formations sédimentaires de la région d'Agades (Républic du Niger): *Mem. Serv. Carte Geol. Als.-Lorr.* **27**, 221 pp.
- Parker, J. M. (1968) Lisbon field area, San Juan County, Utah: in *Natural Gases of North America, Vol. 2*, W. B. Beebe, ed., *Amer. Assoc. Petrol. Geol. Memoir* **9**, 1371–1388.
- Peterson, M. N. A. (1961) Expandable chloritic clay minerals from upper Mississippian carbonate rocks of the Cumberland Plateau in Tennessee: *Amer. Mineral.* **46**, 1245–1269.
- Pettijohn, F. J., Potter, P. E., and Siever, R. (1973) *Sand and Sandstone*: Springer-Verlag, New York, 618 pp.
- Reynolds, R. C. (1980) Interstratified clay minerals: in *Crystal Structures of Clay Minerals and their X-ray Identification*, G. W. Brindley and G. Brown, eds., Mineralogical Soc., London, 249–304.
- Reynolds, R. C. (1983) Calculation of absolute diffraction intensities for mixed-layered clays: *Clays & Clay Minerals* **31**, 233–234.
- Senkayi, A. L., Dixon, J. B., and Hossner, L. R. (1981) Transformation of chlorite to smectite through regularly interstratified intermediates: *Soil Sci. Soc. Amer. J.* **45**, 650–656.
- Shimoda, S. (1969) New data for tosudite: *Clays & Clay Minerals* **17**, 179–184.
- Suchecky, R. K., Perry, E. A., and Hubert, J. F. (1977) Clay petrology of Cambro-Ordovician continental margin, Cow Head klippe, western Newfoundland: *Clays & Clay Minerals* **25**, 163–170.
- Sudo, T. and Hayashi, H. (1956) Types of mixed-layer minerals from Japan: in *Clays and Clay Minerals, Proc. 4th Natl. Conf., University Park, Pennsylvania, 1955*, Ada Swineford, ed., Natl. Acad. Sci. Natl. Res. Council. Publ. **456**, Washington, D.C., 389–412.
- Sudo, T. and Kodama, H. (1957) An aluminum mixed-layer mineral of montmorillonite-chlorite: *Z. Kristallogr.* **109**, 379–387.
- Sudo, T., Takahashi, H., and Matsui, H. (1954) Long spacing of 30 Å from a fireclay: *Nature* **173**, 161.
- Tardy, Y. and Garrels, R. M. (1974) A method of estimating the Gibbs energies of formation of layer silicates: *Geochim. Cosmochim. Acta* **38**, 1101–1116.
- Tompkins, R. E. (1981) Scanning electron microscopy of a regular chlorite/smectite (corrensite) from a hydrocarbon reservoir sandstone: *Clays & Clay Minerals* **29**, 233–235.
- Truesdell, A. H. and Jones, B. F. (1974) WATEQ, a computer program for calculating chemical equilibria of natural waters: *J. Research, U.S. Geol. Surv.* **2**, 233–248.
- Velde, B. (1977) *Clays and Clay Minerals in Natural and Synthetic Systems*: Elsevier, Amsterdam, 218 pp.
- Weaver, C. E. (1984) Origin and geologic implications of the palygorskite deposits of S.E. United States: in *Palygorskite-Septolite Occurrence, Genesis and Uses*, A. Singer and E. Galan, eds., Elsevier, Amsterdam, 39–58.
- Weaver, C. E., Conner, T. G., and Padlan, A. (1982) Geochemistry of Salt No. 6, Gibson dome, Utah, status report, November 1982: Unnumbered BMI/ONWI topical report from Georgia Institute of Technology to Office of Nuclear Waste Isolation, Columbus, Ohio, 47 pp.
- Wood, H. B. (1968) Geology and exploitation of uranium deposits in the Lisbon Valley area, Utah: in *Ore Deposits of the United States, 1933–1967*, J. D. Ridge, ed., American Institute of Mining, Metallurgical and Petroleum Engineers, New York, 770–789.

(Received 6 March 1986; accepted 29 August 1986; Ms. 1568)